

Numerical approximation of convective Brinkman-Forchheimer flow with variable permeability

C. Nwaigwe^{a,*}, J. I. Oahimire^b, A. Weli^a

^aDepartment of Mathematics, Rivers State University, Port Harcourt, Nigeria

^bDepartment of Mathematics, Michael Okpara University of Agriculture, Nigeria

Received 17 July 2022; accepted 25 January 2023

Abstract

This paper investigates the nonlinear dispersion of a pollutant in a non-isothermal incompressible flow of a temperature-dependent viscosity fluid in a rectangular channel filled with porous materials. The Brinkman-Forchheimer effects are incorporated and the fluid is assumed to be variably permeable through the porous channel. External pollutant injection, heat sources and nonlinear radiative heat flux of the Rossland approximation are accounted for. The nonlinear system of partial differential equations governing the velocity, temperature and pollutant concentration is presented in non-dimensional form. A convergent numerical algorithm is formulated using an upwind scheme for the convective part and a conservative-type central scheme for the diffusion parts. The convergence of the scheme is discussed and verified by numerical experiments both in the presence and absence of suction. The scheme is then used to investigate the flow and transport in the channel. The results show that the velocity decreases with increasing suction and Forchheimer parameters, but it increases with increasing porosity. © 2023 University of West Bohemia.

Keywords: Forchheimer flow, nonlinear suction velocity, nonlinear radiation, nonlinear Soret-Dufour effects, variable permeability, variable Soret-Dufour effects

1. Introduction

The Brinkman system is a combination of linear momentum and mass conservation equations for fluid flow in large pores. It is widely used as the basis for studying fluid flow in a wide range of applications, including chemical engineering and pharmaceutical and cosmetic industries. The Forchheimer law accounts for inertial effects in faster flows by including a nonlinear term, but does not account for the Brinkman term [1]. The Brinkman-Forchheimer model adequately models viscous flow in a porous medium and accounts for both inertial and viscous effects.

Convection in porous media is of great interest in areas such as geothermal systems, thermal insulation, nuclear waste disposal and heat exchange systems. The material property, which indicates the ability of fluids to flow through the material, is the permeability. Fluids flow more easily through a material with high permeability. A variation of the permeability of a porous medium may occur due to the orientation of the pores or due to the layered structure of the forming grains of the porous medium [7].

Due to the various applications mentioned above, many researchers have studied related work in the field of porous media flow. The finite element method was used to obtain the solution of the Darcy-Brinkman-Forchheimer equation for an irregular channel flow [14]. The

*Corresponding author. Tel.: +234 803 448 52 74, e-mail: nwaigwe.chinedu@ust.edu.ng.
<https://doi.org/10.24132/acm.2023.767>

nonlinear Brinkman-Forchheimer-extended Darcy flow was investigated by an approximate analytical solution in [5]. Three different physical situations governed by the nonlinear Brinkman-Forchheimer-extended Darcy model were studied. Numerical simulation of flow and heat transfer in a porous medium was investigated by the finite element method in [27] using the nonlinear Darcy-Forchheimer drag force model.

A boundary layer approximation for a closed form solution of the Brinkman-Forchheimer equation was presented in [30]. In [16], a closed form solution of Brinkman-Forchheimer equation is obtained; it involves an elliptic integral and is difficult to apply different boundary conditions. A perturbation method was used to obtain the analytical solution for a fully developed force convection in a porous duct on the basis of the Brinkman-Forchheimer model; however, the validity of the solution is questionable for large values of the Forchheimer number [3]. The Galerkin method was used to analyze the existence and uniqueness of the nonlinear Brinkman-Forchheimer equation in a porous medium [6].

A convective flow over an exponentially stretching sheet embedded in a Darcy-Forchheimer porous medium with heat radiation was investigated by numerical computation using *bvp4c*, a MATLAB program [11]. An implicit-explicit finite difference scheme for the analysis of a channel flow problem was developed by Nwaigwe [20], which studied transportation phenomena with variable cross-diffusion and nonlinear radiation. The present work extends the work of Nwaigwe [20] by incorporating Forchheimer effects, wall velocity suction (nonlinear convection term), variable permeability, nonlinear pollutant injection, exponentially temperature-dependent heat source [32] and an exponentially moving wall velocity. These conditions are in addition to the existing flow and transport conditions, such as nonlinear radiation and the nonlinear Soret-Dufour effects, considered in the original work of Nwaigwe [20]. Moreover, we also extend the numerical scheme in [20] to account for the convective transport through the use of upwind discretization. This endeavor has not been taken before, to best of our knowledge.

Some of the motivations of this work are as follows: In a double-diffusive convection, such as thermohaline, the fluid density depends on both the concentration and temperature [15], leading to their coupling – the cross-diffusion effect. Again, the temperature gradients may in realistic cases result in viscous dissipation and radiation, see also [20]. Hence, a study that incorporates all these effects is essential. Moreover, deriving a mathematical model that describes the combination of these complex processes and proposing, analyzing, implementing and verifying a correct and convergent numerical method for such a complicated mathematical model is a great feat that would serve other researchers who may need such methods for their own models and research. These facts motivate the study.

The non-dimensional form of the mathematical problem is presented in Section 2, while the numerical approximation and convergence analysis are discussed in Section 3. The accuracy and convergence of the proposed scheme are numerically verified for both with ($A_0 \neq 0$) and without suction ($A_0 = 0$) in Section 4. The model is applied to investigate the flow and the results are presented in Section 5. Concluding remarks are made in Section 5.

2. Mathematical formulation of the problem

A nonlinear dispersion of a pollutant in a non-isothermal incompressible flow of a temperature-dependent viscosity fluid in a rectangular channel filled with porous materials is considered. Wall suction velocity and the Brinkman-Forchheimer effects are accounted for and the fluid is considered variably permeable through the porous medium. Further, an external pollutant injection and heat sources are assumed, the radiative heat flux is taken in the complete nonlinear

Rosslund formulation [20]. Nonlinear cross-diffusion effects, viscous dissipation and uniformly applied magnetic field are equally considered. An external heat generation is assumed to follow the Weli and Nwaigwe formulation [32]. At the initial time $t = 0$, the velocity, concentration and temperature are functions of position y . Then, at subsequent times, one of the channel walls is kept stationary and maintained at constant wall temperature and concentration, while the other wall moves exponentially in time, with wall temperature that is sinusoidal in time and with constant wall concentration. With these assumptions, the non-dimensional equations governing the fluid velocity $w(y, t)$ along the channel axis, the pollutant concentration $\phi(y, t)$ and the fluid temperature $\theta(y, t)$ at the lateral point $0 < y < 1$ and time t are given as follows [20]:

$$\frac{\partial w}{\partial t} + a(w) \frac{\partial w}{\partial y} = \frac{\partial}{\partial y} \left(\frac{\partial w}{\partial y} e^{-\alpha \theta} \right) - \frac{e^{-\alpha \theta}}{D_a(y)} w - \frac{C_F}{\sqrt{D_a(y)}} |w| w - Mw + G_T \theta + G_c \phi, \quad (1)$$

$$\frac{\partial \phi}{\partial t} + a(w) \frac{\partial \phi}{\partial y} = \frac{1}{S_c} \frac{\partial}{\partial y} \left(\frac{\partial \phi}{\partial y} e^{\beta \phi} \right) + S_r \frac{\partial}{\partial y} \left(\frac{\partial \theta}{\partial y} e^{\beta \phi} \right) + \gamma_0 \sin^2(\phi^2), \quad (2)$$

$$\begin{aligned} \frac{\partial \theta}{\partial t} + a(w) \frac{\partial \theta}{\partial y} = & \frac{1}{P_r} \frac{\partial}{\partial y} \left[\left(1 + \frac{\lambda \theta}{1000} \right) \frac{\partial \theta}{\partial y} \right] + D_u \frac{\partial}{\partial y} \left(\frac{\partial \phi}{\partial y} e^{\beta \phi} \right) \\ & + \frac{B_r e^{-\alpha \theta}}{P_r} \left(\frac{\partial w}{\partial y} \right)^2 + \frac{R}{P_r} \frac{\partial}{\partial y} \left[\left(\theta + R_2 \right)^3 \frac{\partial \theta}{\partial y} \right] + \gamma e^{-T} \end{aligned} \quad (3)$$

$$\forall (y, t) \in \Omega_{yt} = (0, 1) \times (0, T_f < \infty),$$

subject to

$$w(y, 0) = (0.1 + \alpha_w)y, \quad \phi(y, 0) = 0.8y, \quad \theta(y, 0) = 1 + y(1 - y) \quad \forall y \in \bar{\Omega}_y = [0, 1] \quad (4)$$

and

$$\begin{aligned} w(0, t) = 0, \quad w(1, t) = 0.1 + \alpha_w e^{-t}, \\ \phi(0, t) = 0, \quad \phi(1, t) = 0.8, \\ \theta(0, t) = 1, \quad \theta(1, t) = 0.5 + R_2 \sin(t) + 0.5 \cos(t) \quad \forall t \in \bar{\Omega}_t = [0, T_f < \infty], \end{aligned} \quad (5)$$

where

$$\begin{aligned} a(w) &= A_0 e^{-(1+w^2)t}, \\ D_a(y) &= D_{\hat{a}} + e_p e^{-y} \end{aligned} \quad (6)$$

are the suction velocity and variable permeability functions. Other parameters appearing in (1)–(6) are specified as:

A_0 – suction parameter	β – diffusivity variation parameter
e_p – permeability variation parameter	P_r – Prandtl number
γ – heat source parameter	D_u – Dufour coefficient
α – viscosity variation parameter	C_F – Forchheimer number
M – magnetic field parameter	γ_0 – injection parameter
$D_{\hat{a}}$ – Darcy number	B_r – Brinkman number
G_T – thermal Grashof number	R – thermal radiation parameter
G_c – solutal Grashof number	R_2 – nonlinear radiation parameter
S_c – Schmidt number	λ – thermal conductivity variation parameter
S_r – Soret coefficient	α_w – wall velocity coefficient

A detailed derivation and expressions for the non-dimensional parameters can be found in [20].

Equations (1)–(5) form a system of coupled nonlinear partial differential equations, whose exact analytical solution cannot be found. Therefore, a numerical scheme to approximate the solution is proposed in the next section.

3. Numerical scheme and analysis

The numerical procedure for approximating the solution of the proposed model is presented in this section. The scheme is an extension of the implicit-explicit scheme published in [20]. The convergence of the scheme is also discussed.

3.1. Formulation of the scheme

We choose $N_y > 1$ as a positive integer and define the mesh

$$\Omega_h = \{y_i | y_i = ih, h = 1/N_y, i = 0, 1, \dots, N_y\}.$$

Let Δt and N_t be given such that $N_t = T/\Delta t$ is a positive integer and $t^n := n\Delta t$ for $n = 0, 1, \dots, N_t$. We seek the following approximations for the grid point solution values:

$$w_i^n \approx w(y_i, t^n), \quad \phi_i^n \approx \phi(y_i, t^n), \quad \theta_i^n \approx \theta(y_i, t^n).$$

To obtain a stable discretization of the convective terms $a(w) \frac{\partial w}{\partial y}$, etc., we define the following single-sign quantities:

$$a(w)^\pm = \frac{1}{2}(a(w) \pm |a(w)|). \quad (7)$$

Observe that $a(w)^+ \geq 0$, while $a(w)^- \leq 0$. For convenience purposes, we define the following function [20]:

$$\Psi(\theta) = 1 + \frac{\lambda\theta}{1000} + (\theta + R_2)^3 R, \quad (8)$$

which will allow us to rewrite the sum of the first and fourth terms on the right hand side of (3) to the following compact form:

$$\frac{1}{P_r} \frac{\partial}{\partial y} \left[\left(1 + \frac{\lambda\theta}{1000} \right) \frac{\partial \theta}{\partial y} \right] + \frac{R}{P_r} \frac{\partial}{\partial y} \left[(\theta + R_2)^3 \frac{\partial \theta}{\partial y} \right] \equiv \frac{1}{P_r} \frac{\partial}{\partial y} \left(\Psi \frac{\partial \theta}{\partial y} \right). \quad (9)$$

Also, we define the following notations for the grid point values for the transport properties

$$\Gamma_i^n := e^{\alpha\phi_i^n}, \quad \eta_i^n := e^{\beta\phi_i^n}, \quad \Psi_i^n := \Psi(\theta_i^n)$$

and the discrete derivative operators

$$\delta^\pm u_i = u_{i\pm 1} - u_i.$$

Moreover, we use the short forms for the value of the transport properties at intermediate grid points

$$\Pi_{i\pm 1/2}^n := \frac{\Pi_i^n + \Pi_{i\pm 1}^n}{2} \quad \text{for } \Pi = \Gamma, \eta, \Psi.$$

Therefore, we extend the scheme from [20] by incorporating the discrete convective and source terms [32]. The convective (first derivative) term is discretized by using an upwind approach [9, 10, 17, 28, 29, 32], while the diffusion (second derivative) is approached by freezing coefficients [20], see also [4, 8, 12, 13, 18, 19, 26]. The Forchheimer term is discretized by freezing the non-positive coefficient at the previous time level t^n , while the velocity factor is evaluated at the new time level t^{n+1} . This follows the same philosophy in the diffusion terms and the purpose is to ensure stability of the resulting scheme. The source terms in the concentration and heat equations are all evaluated at time levels t^n . These lead to the following schemes for the three governing equations:

velocity scheme

$$\begin{aligned}
 w_i^{n+1} + \Delta t \frac{w_i^{n+1} - w_{i-1}^{n+1}}{\Delta y} a(w_i^n)^+ + \Delta t \frac{w_{i+1}^{n+1} - w_i^{n+1}}{\Delta y} a(w_i^n)^- \\
 = \Delta t \left[\frac{\Gamma_{i-1/2}^n}{(\Delta y)^2} \delta^- + \frac{\Gamma_{i+1/2}^n}{(\Delta y)^2} \delta^+ - \frac{\Gamma_i^n}{D_a(y_i)} - M \right] w_i^{n+1} + w_i^n + \Delta t (G_T \theta_i^n + G_c \phi_i^n) \\
 - \Delta t \frac{C_F}{\sqrt{D_a(y_i)}} |w_i^n| w_i^{n+1} \quad \forall (i, n),
 \end{aligned} \tag{10}$$

concentration scheme

$$\begin{aligned}
 \phi_i^{n+1} + \Delta t \frac{\phi_i^{n+1} - \phi_{i-1}^{n+1}}{\Delta y} a(w_i^n)^+ + \Delta t \frac{\phi_{i+1}^{n+1} - \phi_i^{n+1}}{\Delta y} a(w_i^n)^- \\
 = \frac{\Delta t}{(\Delta y)^2 S_c} (\eta_{i-1/2}^n \delta^- + \eta_{i+1/2}^n \delta^+) \phi_i^{n+1} + \frac{\Delta t S_r}{(\Delta y)^2} (\eta_{i-1/2}^n \delta^- + \eta_{i+1/2}^n \delta^+) \theta_i^n \\
 + \Delta t \gamma_0 \sin^2((\phi_i^n)^2) + \phi_i^n \quad \forall (i, n),
 \end{aligned} \tag{11}$$

temperature scheme

$$\begin{aligned}
 \theta_i^{n+1} + \Delta t \frac{\theta_i^{n+1} - \theta_{i-1}^{n+1}}{\Delta y} a(w_i^n)^+ + \Delta t \frac{\theta_{i+1}^{n+1} - \theta_i^{n+1}}{\Delta y} a(w_i^n)^- \\
 = \frac{\Delta t}{(\Delta y)^2 P_r} (\Psi_{i-1/2}^n \delta^- + \Psi_{i+1/2}^n \delta^+) \theta_i^{n+1} + \frac{\Delta t D_u}{(\Delta y)^2} (\eta_{i-1/2}^n \delta^- + \eta_{i+1/2}^n \delta^+) \phi_i^n + \theta_i^n \\
 + \frac{\Delta t B_r}{P_r} \Gamma_i^n \left(\frac{w_{i+1}^n - w_{i-1}^n}{2\Delta y} \right)^2 + \gamma e^{T_i^n} \quad \forall (i, n),
 \end{aligned} \tag{12}$$

subject to the following initial and boundary conditions:

$$\begin{aligned}
 w_i^0 = (0.1 + \alpha_w) y_i, \quad \phi_i^0 = 0.8 y_i, \quad T_i^0 = 1 + (1 - y_i) y_i \quad \forall y_i \in \Omega_h, \\
 w_0^{n+1} = 0, \quad w_{N_y}^{n+1} = 0.1 + \alpha_w e^{-t^{n+1}}, \quad \phi_0^{n+1} = 0, \quad \phi_{N_y}^{n+1} = 0.8 \quad \forall n, \\
 \theta_0^{n+1} = 1, \quad \theta_{N_y}^{n+1} = 0.5 + R_2 \sin(t^{n+1}) + 0.5 \cos(t^{n+1}) \quad \forall n.
 \end{aligned} \tag{13}$$

3.2. Convergence analysis

The scheme proposed in (10)–(13) can be easily shown to converge to the exact solution of (1)–(5) as we briefly discuss below. The numerical verification of this convergence property is detailed in the next section via a grid convergence analysis.

In the case of no convective terms, it was rigorously proved in [20] that the scheme (10)–(13) converges with second order in space and first order in time. Hence, the remaining condition to guarantee that the scheme is consistent, stable and convergent is to prove that the proposed upwind discretization

$$\frac{w_i^{n+1} - w_{i-1}^{n+1}}{\Delta y} a(w_i^n)^+ + \frac{w_{i+1}^{n+1} - w_i^{n+1}}{\Delta y} a(w_i^n)^-$$

for the convective term $a(w_i^n) \frac{\partial w}{\partial y}$ is consistent, stable and also convergent. However, it is a known and easily provable result in numerical analysis (see, e.g., [2, 9, 10, 28, 29]) that the upwind discretization of the first derivative is consistent, stable and has first order of convergence in space, see also the recent paper [32]. Furthermore, since the coefficient in the first derivative term is frozen (evaluated at time level t^n), it means that the scheme is also first order in time, see [32] for a proof of this. Therefore, we conclude that the scheme presented above is (i) first order in both space and time when the convective term is present, but (ii) it is second order in space and first order in time if the convective term is ignored. These convergence properties are verified in the next section.

4. Numerical verification

This section verifies the proposed numerical scheme for both accuracy and convergence using numerical test cases with ($A_0 \neq 0$) and without ($A_0 = 0$) suction. The scheme is implemented in an in-house C++ code developed and maintained by the first author of the paper and has been extensively validated in earlier studies, see, e.g., [20–22, 31] and [32]. The following data is used for the verification: $\alpha = 1.0$, $S_c = 1.0$, $\beta = 1.0$, $S_r = 0.0001$, $P_r = 0.75$, $\lambda = 0.000001$, $D_u = 0.0001$, $R = 0.01$, $R_2 = 1.0$, $\alpha_w = 1.0$, $D_{\hat{a}} = 0.1$, $M = 1.0$, $G_T = 1.0$, $G_c = 1.0$, $B_r = 0.1$, $\gamma = 1.0$, $\gamma_0 = 1.0$, $C_F = 1.0$, $e_p = 1.0$, $\Delta t = 0.005$. For no suction, we set $A_0 = 0$, while the case with suction uses $A_0 = 1.0$.

The method of manufactured solutions is adopted [20, 21, 24, 25]; hence, we consider the model equations with the functions $f_w(y, t)$, $f_\phi(y, t)$ and $f_\theta(y, t)$ added to the right hand side of (1), (2) and (3), respectively, where

$$\begin{aligned} f_w(y, t) &= -\pi A_0 e^{-t} e^{-t[1+e^{-2t} \cos^2(\pi y)]} \sin(\pi y) - G_c e^{-t-y^2} - G_T e^{-ty} \\ &\quad + \pi \alpha t e^{-t} e^{-\alpha e^{-ty}} e^{-ty} \sin(\pi y) + \left[M + \frac{C_F e^{-re(t)} |\cos(\pi y)|}{\sqrt{D_a + e_p e^{-y}}} + \frac{e^{-\alpha e^{-ty}}}{D_a + e_p e^{-y}} \right] e^{-t} \cos(\pi y) \\ &\quad - e^{-t} \cos(\pi y) + \pi^2 e^{-t} e^{-\alpha e^{-ty}} \cos(\pi y), \\ f_\phi(y, t) &= -2A_0 y e^{t[-1-e^{-2t} \cos^2(\pi y)]} e^{-t-y^2} - S_r \left(2\beta t y e^{\beta e^{-t-y^2}} e^{-ty} e^{-t-y^2} + t^2 e^{\beta e^{-t-y^2}} e^{-ty} \right) \\ &\quad - \gamma_0 \sin^2(e^{-2t-2y^2}) - e^{-t-y^2} \\ &\quad - \frac{1}{S_c} \left(4\beta y^2 e^{\beta e^{-t-y^2}} e^{-2t-2y^2} + 4y^2 e^{\beta e^{-t-y^2}} e^{-t-y^2} - 2e^{\beta e^{-t-y^2}} e^{-t-y^2} \right), \\ f_\theta(y, t) &= -A_0 t e^{-ty} e^{t[-1-e^{-2t} \cos^2(\pi y)]} - \frac{1}{P_r} \left[\pi^2 B_r e^{-2t} e^{-\alpha e^{-ty}} \sin^2(\pi y) \right] \\ &\quad - D_u \left(4\beta y^2 e^{\beta e^{-t-y^2}} e^{-2t-2y^2} + 4y^2 e^{\beta e^{-t-y^2}} e^{-t-y^2} - 2e^{\beta e^{-t-y^2}} e^{-t-y^2} \right) - \gamma e^{-e^{-ty}} - y e^{-ty} \\ &\quad - \left\{ t^2 \left[R (R_2 + e^{-ty})^3 + 0.001 \lambda_1 + 1 \right] + t \left[3Rt (R_2 + e^{-ty})^2 e^{-ty} + 0.001 \lambda_1 t e^{-ty} \right] \right\} \frac{e^{-ty}}{P_r}. \end{aligned}$$

Further, we impose the initial and boundary conditions

$$w(y, 0) = \cos(\pi y), \quad \phi(y, 0) = e^{-y^2}, \quad \theta(y, 0) = 1 \tag{14}$$

and

$$\begin{aligned} w(0, t) &= e^{-t}, & \phi(0, t) &= e^{-t}, & \theta(0, t) &= 1, \\ w(1, t) &= \cos(\pi)e^{-t}, & \phi(1, t) &= e^{-1-t}, & \theta(1, t) &= e^{-ty}. \end{aligned} \tag{15}$$

Given the above initial-boundary value problem, it can be easily verified that the exact solution is

$$w(y, t) = \cos(\pi y)e^{-t}, \quad \phi(y, t) = e^{-(y^2+t)}, \quad \theta(y, t) = e^{-ty}. \tag{16}$$

The proposed scheme is used to solve the above problem. We compute the solutions on a sequence of 2^s grid points ($s = 1, 2, \dots, 9$) and for both $A_0 = 0$ (no convective transport) and $A_0 = 1.0$ (with convection). The time step is computed as $\Delta t = h^2/2$, where h is the mesh size. The error, in L_2 norm, and the experimental order of convergence (EOC) are computed and tabulated for each flow variable. The results for convective transport and non-convective transport are shown in Tables 1 and 2, respectively. It is obvious that the numerical solution converges

Table 1. Experimental order of convergence (EOC) for the convective case: E_w, E_ϕ and E_θ are two-norm errors in w, ϕ and θ , respectively, while EOC_w, EOC_ϕ and EOC_θ are the computed orders of convergence

M	E_w	EOC_w	E_ϕ	EOC_ϕ	E_θ	EOC_θ
2	0	–	0	–	0	–
4	$1.73772e-2$	–	$3.22185e-3$	–	$1.98031e-3$	–
8	$1.17385e-2$	0.565945	$1.63310e-3$	0.980277	$8.22406e-4$	1.26780
16	$6.66118e-3$	0.817403	$8.29555e-4$	0.977205	$3.62755e-4$	1.18086
32	$3.50349e-3$	0.926985	$4.14255e-4$	1.001820	$1.61014e-4$	1.17181
64	$1.79464e-3$	0.965100	$2.06949e-4$	1.001240	$7.49172e-5$	1.10382
128	$9.07616e-4$	0.983537	$1.03375e-4$	1.001390	$3.59150e-5$	1.06071
256	$4.56373e-4$	0.991871	$5.16613e-5$	1.000730	$1.75629e-5$	1.03206
512	$2.28820e-4$	0.995998	$2.58233e-5$	1.000410	$8.68044e-6$	1.01669

Table 2. Experimental order of convergence (EOC) for the non-convective case: E_w, E_ϕ and E_θ are two-norm errors in w, ϕ and θ , respectively, while EOC_w, EOC_ϕ and EOC_θ are the computed orders of convergence

M	E_w	EOC_w	E_ϕ	EOC_ϕ	E_θ	EOC_θ
2	0	–	0	–	0	–
4	$6.00310e-3$	–	$7.86879e-4$	–	$1.88544e-3$	–
8	$1.68373e-3$	1.83405	$1.96969e-4$	1.99818	$4.91980e-4$	1.93823
16	$4.42714e-4$	1.92721	$4.86849e-5$	2.01642	$1.26275e-4$	1.96203
32	$1.11310e-4$	1.99180	$1.21331e-5$	2.00453	$3.16213e-5$	1.99760
64	$2.79065e-5$	1.99590	$3.03033e-6$	2.00140	$7.91623e-6$	1.99801
128	$6.97906e-6$	1.99950	$7.57426e-7$	2.00030	$1.97925e-6$	1.99986
256	$1.74507e-6$	1.99975	$1.89345e-7$	2.00009	$4.94856e-7$	1.99988
512	$4.36278e-7$	1.99997	$4.73353e-8$	2.00003	$1.23714e-7$	2.00000

to the exact solution in both cases and at the correct orders of convergence; namely, first order for the convective case and second order for the non-convective case. This observation verifies theoretical convergence results as concluded in Section 3.2. Hence, the proposed algorithm and its implementation can be used to correctly simulate the flow problem being investigated in this study.

5. Application

This section presents the results of the application of the scheme to a flow problem. The velocity profiles are discussed in Section 5.1, those of concentration and temperature are jointly discussed in Sections 5.2 and 5.3, respectively.

5.1. Velocity variations

Fig. 1 illustrates the variation of velocity profile with different values of the Forchheimer parameter (at $t = 0.5$). The results show that an increase in the Forchheimer parameter led to a decrease in the velocity profile throughout the domain. Fig. 2 shows the effect of the permeability parameter on the velocity profile (at $t = 1.0$). It is obvious that as the permeability parameter increases, the velocity increases which is not surprising, because when the pores of a porous medium are larger, the resistance to flow reduces. Fig. 3 displays the influence of the suction parameter on the velocity distribution (at $t = 0.5$). The effect of increasing suction parameter is to decrease the velocity. This is another physically realistic result because suction causes fluid to be drawn into the pores of the channel wall, which is perpendicular to the direction of the main flow direction (along the channel axis), thus, leading to a reduction in the main flow. These results are in agreement with those presented in [23].

5.2. Concentration

Figs. 4–8 depict the variation of concentration profiles for various parameters. Fig. 4 shows that the effect of increasing suction parameter (at $t = 1.0$) is to decrease the concentration of the pollutant, while Fig. 5 shows that the concentration of the pollutant (at $t = 1.0$) increases as the diffusivity parameter increases. In Fig. 6, it can also be seen that an increase in the Soret parameter (at $t = 0.25$) led to a decrease in the concentration. Other observations include

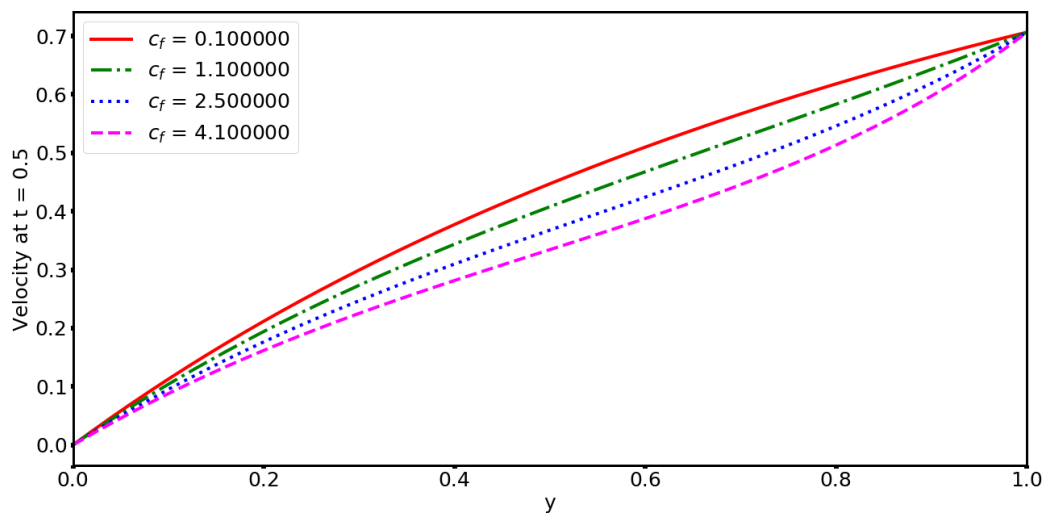


Fig. 1. Variation in velocity with the change of the Forchheimer parameter C_F

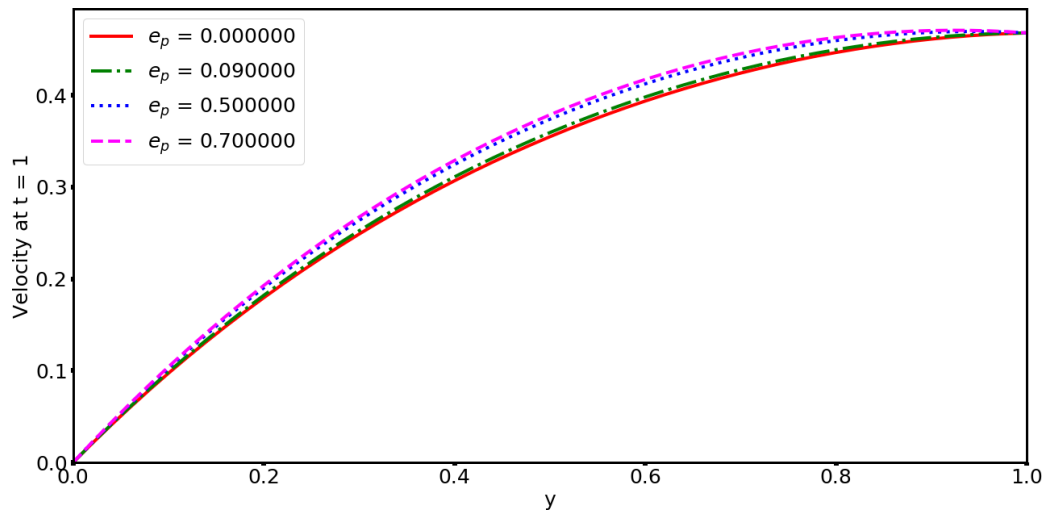


Fig. 2. Variation in velocity with the change of the permeability variation parameter e_p

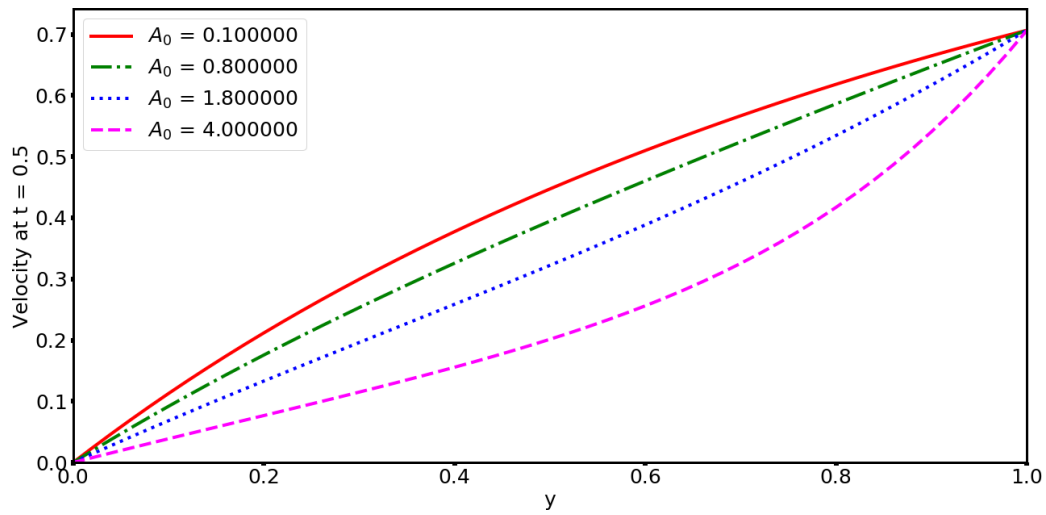


Fig. 3. Effect of the suction parameter A_0 on the velocity profile

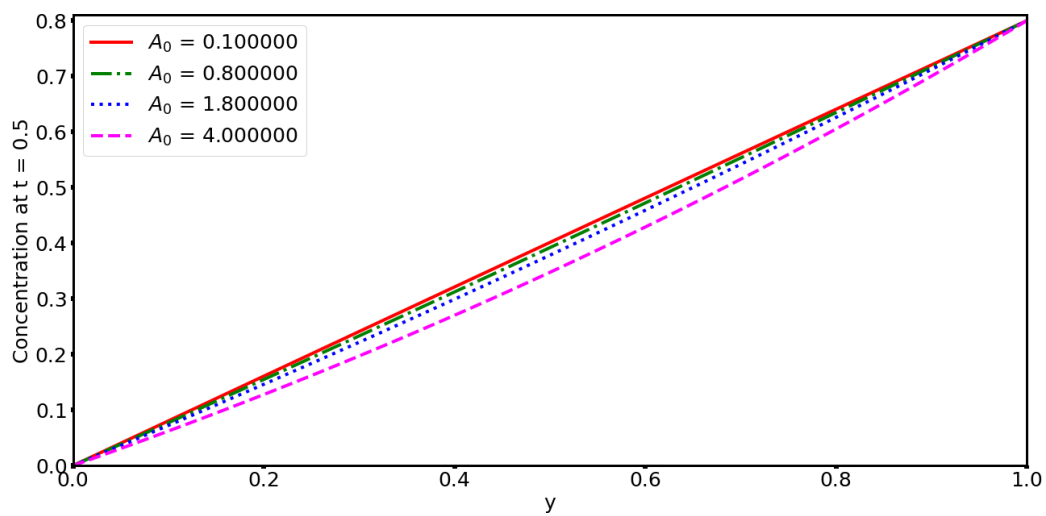


Fig. 4. Effect of the suction parameter A_0 on the concentration profile

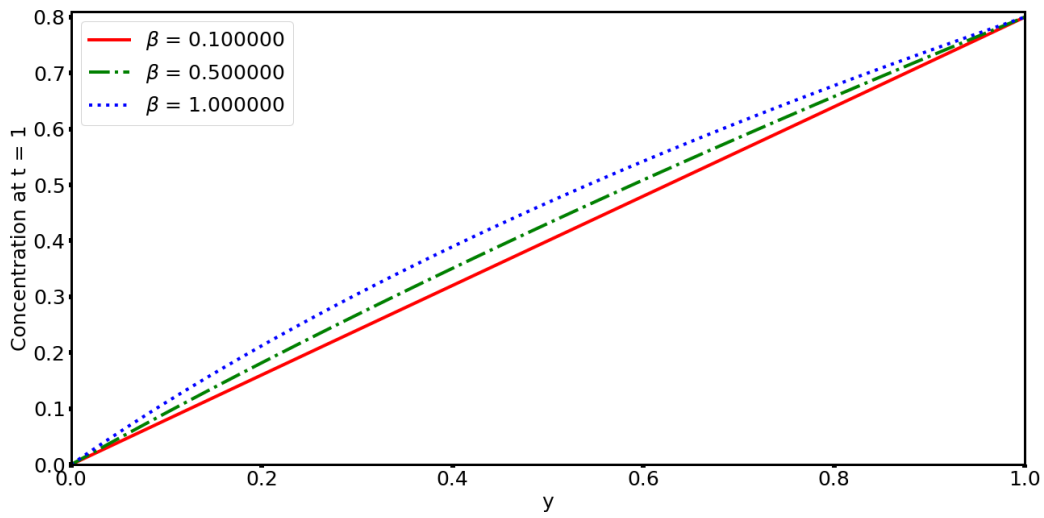


Fig. 5. Effect of the diffusivity variation parameter β on the concentration profile

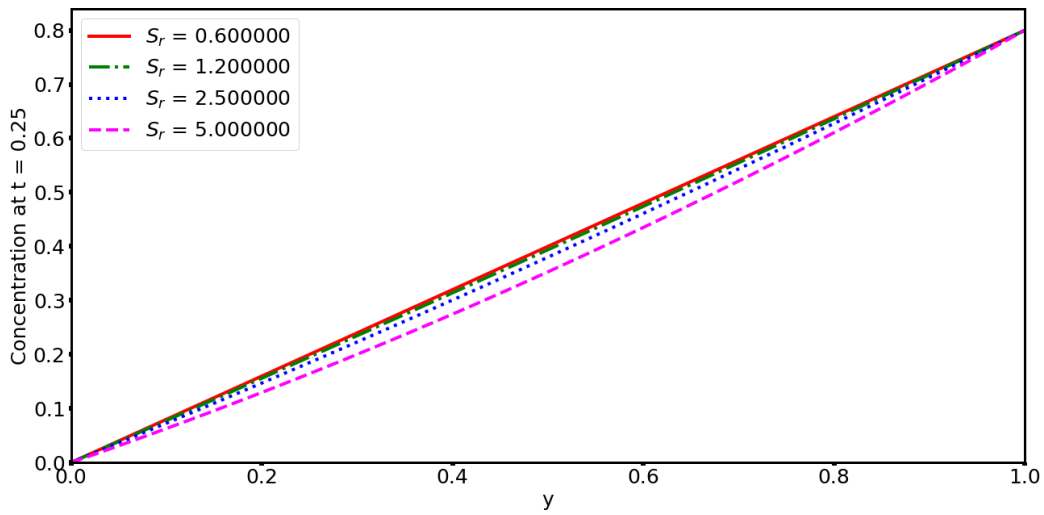


Fig. 6. Effect of the Soret parameter S_r on the concentration profile

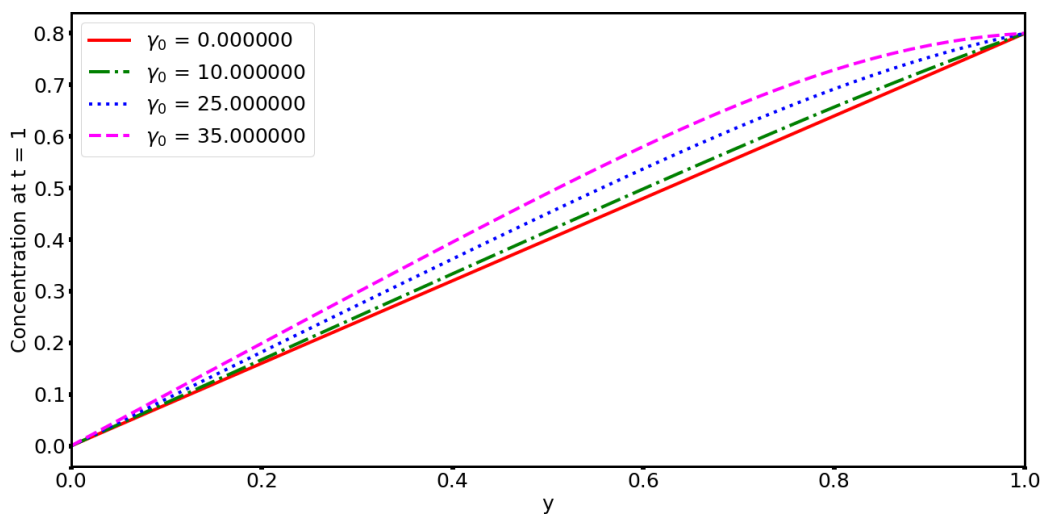


Fig. 7. Effect of the pollutant injection parameter γ_0 on the concentration profile

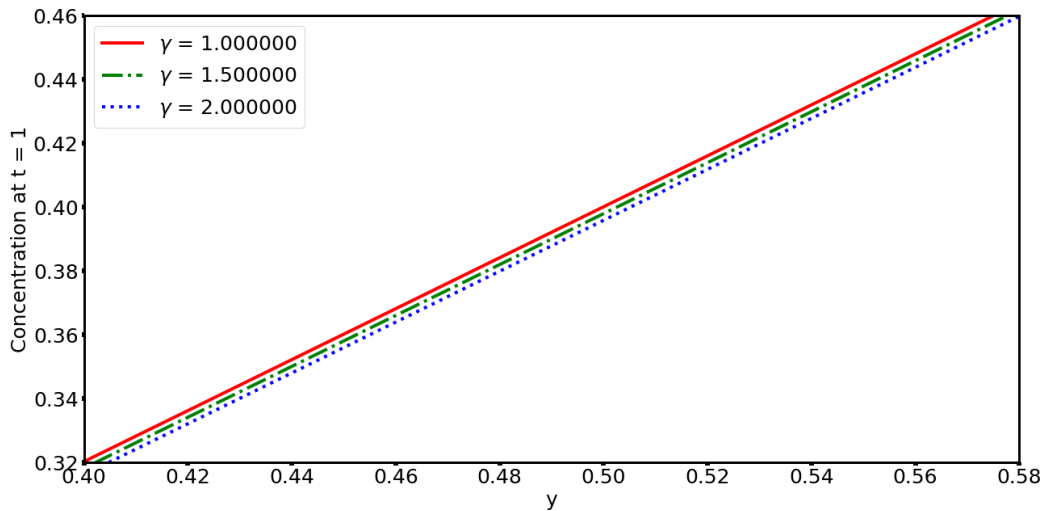


Fig. 8. Effect of the heat source parameter γ on the concentration profile

that the concentration (at $t = 1.0$) increases as the pollutant injection parameter increases – a very realistic result, see Fig. 7, and an increase in the heat source parameter (at $t = 1.0$) leads to a decrease in the concentration, Fig. 8, but this effect is mostly observed away from the channel walls. This behavior also follows the physics in the sense that heat sources increase the internal energy of the fluid, which in turn increases the diffusion of the pollutant (due to cross-diffusion), thereby decreasing concentration. This has application in engineering systems, where substances are injected into a fluid system to avoid corrosion. Then, heat can be injected to cleanse the fluid of a substance.

5.3. Temperature variations

Figs. 9–15 demonstrate the influence of various flow parameters on the temperature profile. Fig. 9 shows that the fluid temperature decreases as the Forchheimer parameter increases, while Fig. 10 depicts that an increase in the suction parameter leads to a decrease in the fluid temperature in the region close to the stationary wall ($y = 0$), but increases in the region near the mobile wall ($y = 1$). It is also observed that the temperature of the fluid increases due to increase in

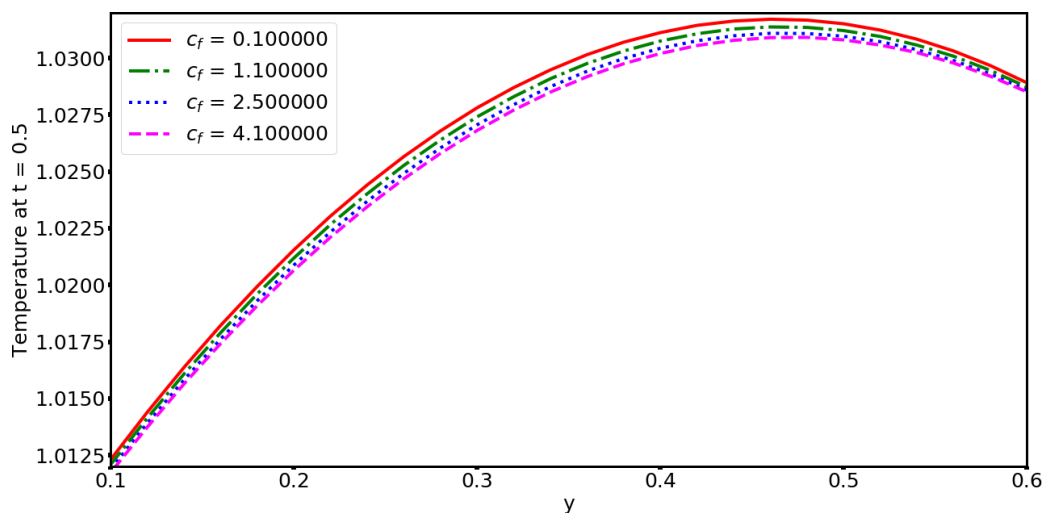


Fig. 9. Effect of the Forchheimer parameter C_F on the temperature profile

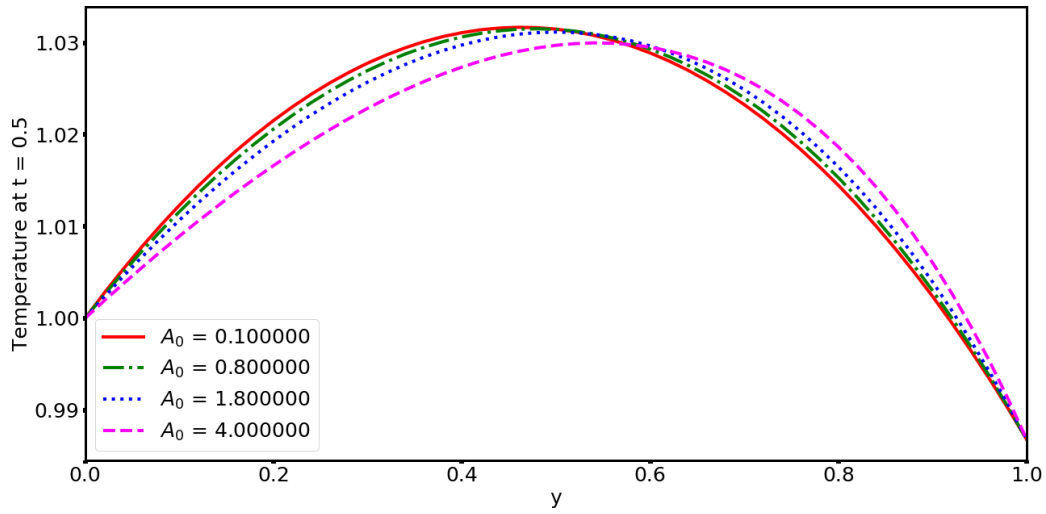


Fig. 10. Effect of the suction parameter A_0 on the temperature profile

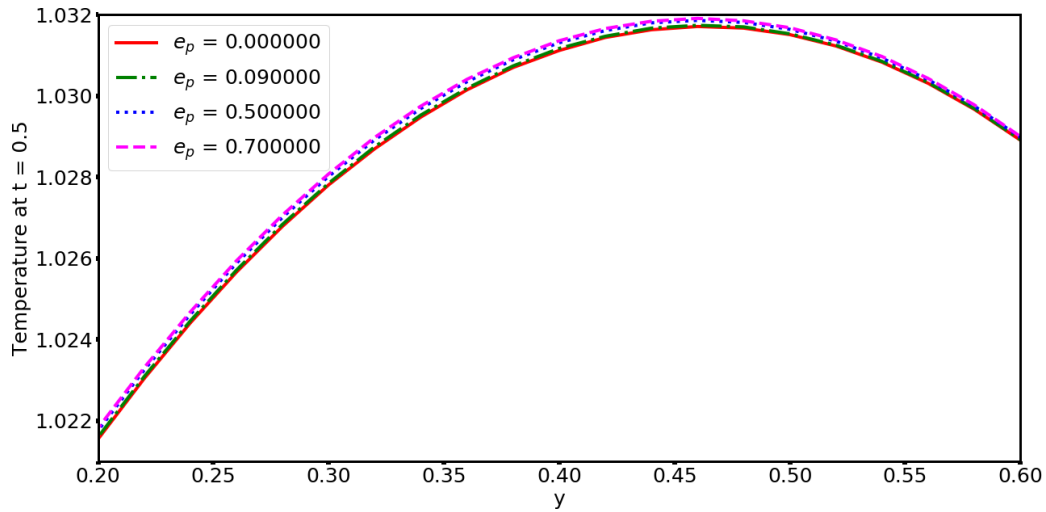


Fig. 11. Effect of the permeability variation parameter e_p on the temperature profile

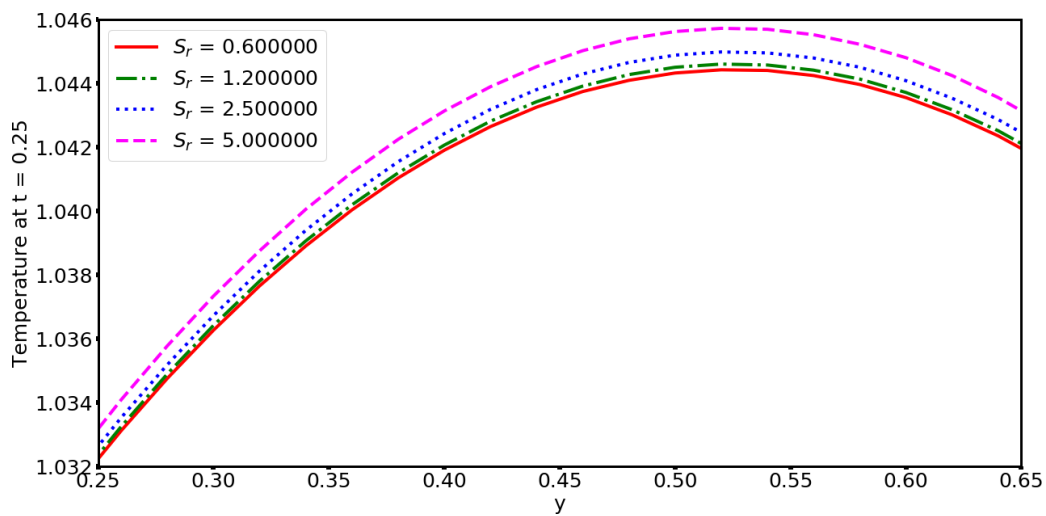


Fig. 12. Effect of the Soret parameter S_r on the temperature profile

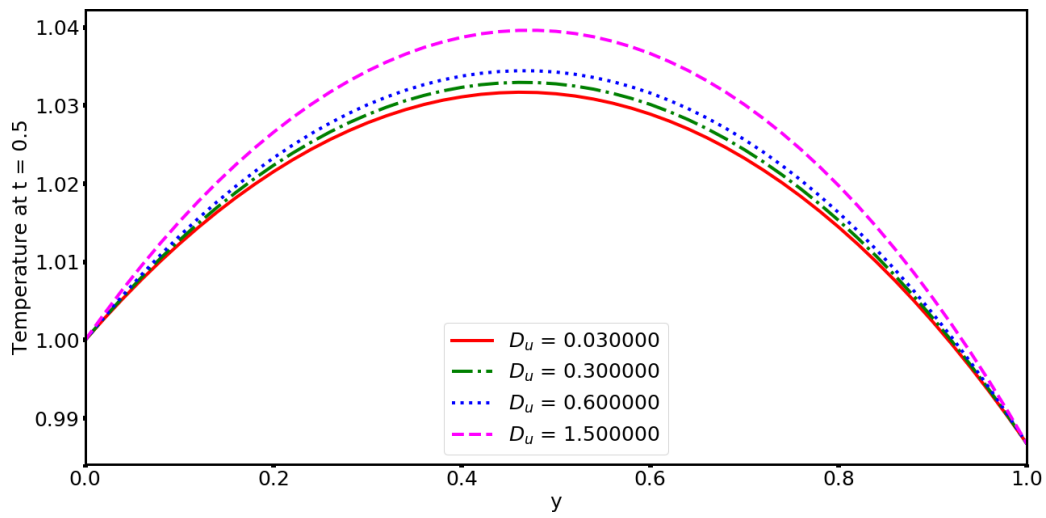


Fig. 13. Effect of the Dufour parameter D_u on the temperature profile

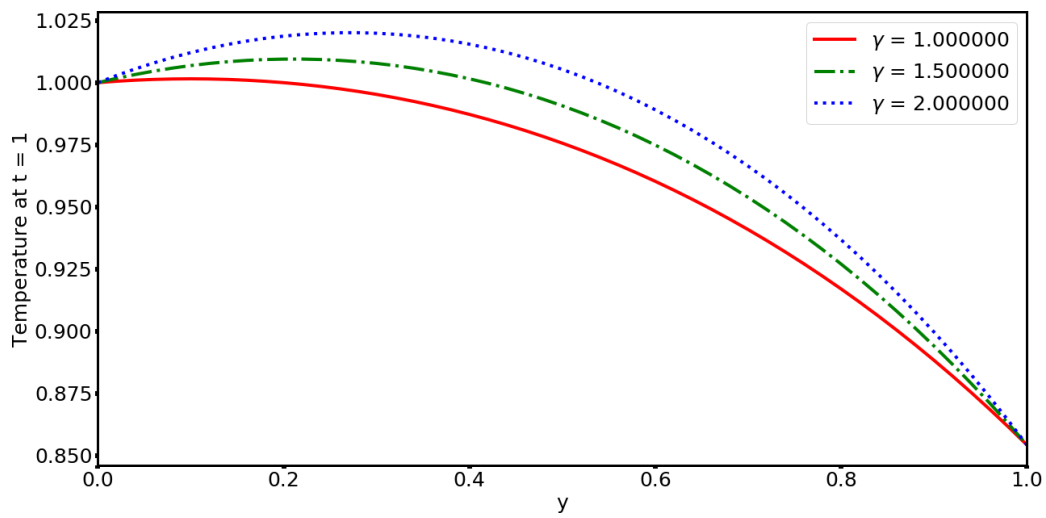


Fig. 14. Effect of the heat source parameter γ on the temperature profile

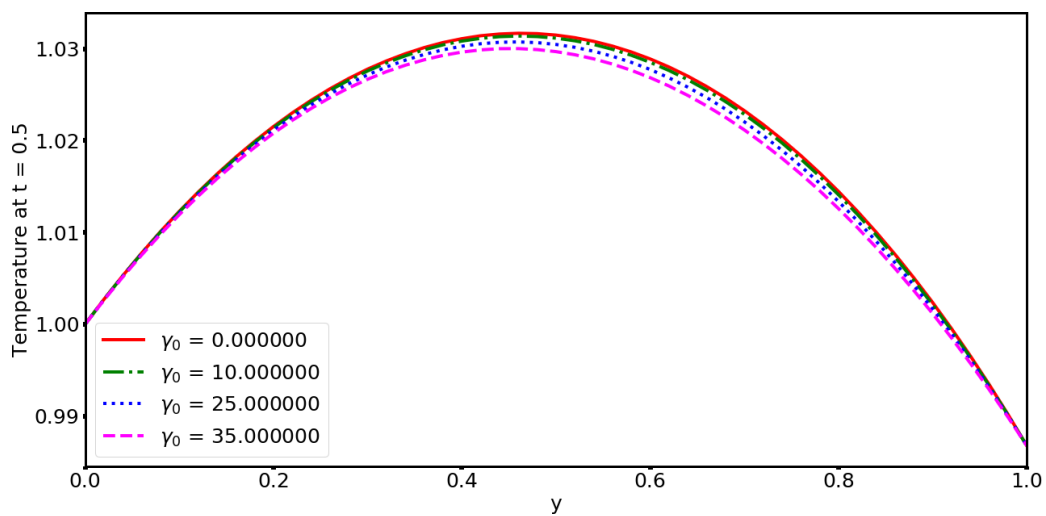


Fig. 15. Effect of the pollutant injection parameter γ_0 on the temperature profile

the permeability parameter, see Fig. 11. An increase in the Soret parameter led to an increase in the fluid temperature, Fig. 12, which is to be expected, because the Soret parameter is associated with the mass flux caused by the temperature gradient. The same effect is observed in Fig. 13 when increasing the Dufour parameter. The effect of increasing heat source parameter is to increase the temperature of the fluid, Fig. 14. This is also realistic since more addition of heat should naturally increase the temperature. Finally, we also observed that an increase in the pollutant injection parameter resulted in the decrease in temperature of fluid flow, see Fig. 15. These results are in agreement with those presented [18].

6. Conclusions

The process of heat and mass transfer in a porous channel flow of a fluid with nonlinear transport properties, variable permeability, nonlinear suction and nonlinear cross-diffusion was investigated. The problem led to a nonlinear system of convection-diffusion-reaction equations, which was numerically solved using upwind and conservative-type central schemes. The investigation of the flow revealed that

- (i) increasing the permeability parameter increases the fluid velocity,
- (ii) increase in the suction parameter led to the decrease in fluid velocity and
- (iii) increasing the suction parameter led to the decrease in pollutant concentration.

Acknowledgement

The first author is grateful to the Petroleum Technology Development Fund (PTDF), Nigeria for funding his Ph.D. at the University of Warwick, UK during 2012–2016.

References

- [1] Avramenko, A. A., Shevchuk, I. V., Kovetskaya, M. M., Kovetska, Y. Y., Darcy-Brinkman-Forchheimer model for film boiling in porous media, *Transport in Porous Media* 134 (3) (2020) 503–536. <https://doi.org/10.1007/s11242-020-01452-7>
- [2] Ferziger, J. H., Perić, M., *Computational methods for fluid dynamics*, Edition 3, Springer, 2002. <https://doi.org/10.1007/978-3-642-56026-2>
- [3] Hooman, K., A perturbation solution for forced convection in a porous-saturated duct, *Journal of Computational and Applied Mathematics* 211 (1) (2008) 57–66. <https://doi.org/10.1016/j.cam.2006.11.005>
- [4] Hundsdorfer, W., Verwer, J., *Numerical solution of time-dependent advection-diffusion-reaction equations*, Springer Science and Business Media, 2013. <https://doi.org/10.1007/978-3-662-09017-6>
- [5] Jha, B. K., Kaurangini, M. L., Approximate analytical solution for non-linear Brinkman-Forchheimer-extended Darcy flow model, *Applied Mathematics* 2 (12) (2011) 1432–1436. <https://doi.org/10.4236/am.2011.212202>
- [6] Kaloni, P., Guo, J., Steady nonlinear double-diffusive convection in a porous medium based upon the Brinkman-Forchheimer model, *Journal of Mathematical Analysis and Applications* 204 (1) (1996) 138–155. <https://doi.org/10.1006/jmaa.1996.0428>
- [7] Karmakar, T., Reza, M., Sekhar, G. R., Forced convection in a fluid saturated anisotropic porous channel with isoflux boundaries, *Physics of Fluids* 31 (11) (2019) 1–12. <https://doi.org/10.1063/1.5126892>
- [8] Kuzmin, D., *A guide to numerical methods for transport equations*, University of Erlangen-Nuremberg, 2010 (<http://www.mathematik.uni-dortmund.de/~kuzmin/Transport.pdf>).

- [9] LeVeque, R. J., Numerical methods for conservation laws, Birkhäuser Basel, 1992. <https://doi.org/10.1007/978-3-0348-8629-1>
- [10] LeVeque, R. J., Finite volume methods for hyperbolic problems, Volume 31, Cambridge University Press, 2002. <https://doi.org/10.1017/CBO9780511791253>
- [11] Lund, L. A., Omar, Z., Khan, I., Darcy-Forchheimer porous medium effect on rotating hybrid nanofluid on a linear shrinking/stretching sheet, *International Journal of Numerical Methods for Heat & Fluid Flow* 31 (12) (2021) 3621–3641. <https://doi.org/10.1108/HFF-11-2020-0716>
- [12] Matus, P., Gaspar, F., Hieu, L. M., Tuyen, V. T. K., Monotone difference schemes for weakly coupled elliptic and parabolic systems, *Computational Methods in Applied Mathematics* 17 (2) (2017) 287–298. <https://doi.org/10.1515/cmam-2016-0046>
- [13] Matus, P., Hieu, L. M., Vulkov, L. G., Analysis of second order difference schemes on non-uniform grids for quasilinear parabolic equations, *Journal of Computational and Applied Mathematics* 310 (2017) 186–199. <https://doi.org/10.1016/j.cam.2016.04.006>
- [14] Murali, K., Naidu, V. K., Venkatesh, B., Solution of Darcy-Brinkman-Forchheimer equation for irregular flow channel by finite elements approach, *Journal of Physics: Conference Series* 1172 (2019) 1–14. <https://doi.org/10.1088/1742-6596/1172/1/012033>
- [15] Nield, D. A., Bejan, A., Convection in porous media, Springer Cham, 2017. <https://doi.org/10.1007/978-3-319-49562-0>
- [16] Nield, D. A., Junqueira, S. L. M., Lage, J. L., Forced convection in a fluid-saturated porous-medium channel with isothermal or isoflux boundaries, *Journal of Fluid Mechanics* 322 (1996) 201–214. <https://doi.org/10.1017/S0022112096002765>
- [17] Nwaigwe, C., Coupling methods for 2D/1D shallow water flow models for flood simulations, Ph.D. thesis, University of Warwick, United Kingdom, 2016.
- [18] Nwaigwe, C., Analysis and application of a convergent difference scheme to nonlinear transport in a Brinkman flow, *International Journal of Numerical Methods for Heat & Fluid Flow* 30 (10) (2020) 4453–4473. <https://doi.org/10.1108/HFF-10-2019-0758>
- [19] Nwaigwe, C., Sequential implicit numerical scheme for pollutant and heat transport in a plane-Poiseuille flow, *Journal of Applied and Computational Mechanics* 6 (1) (2020) 13–25.
- [20] Nwaigwe, C., Mathematical modeling and numerical analyses of transport phenomena with variable cross-diffusion and nonlinear radiation, *Computational Thermal Sciences: An International Journal* 13 (1) (2021) 73–96. <https://doi.org/10.1615/ComputThermalScien.2020033936>
- [21] Nwaigwe, C., Makinde, O. D., Finite difference investigation of a polluted non-isothermal variable-viscosity porous media flow, *Diffusion Foundations* 26 (2020) 145–156. <https://doi.org/10.4028/www.scientific.net/DF.26.145>
- [22] Nwaigwe, C., Weli, A., Makinde, O. D., Computational analysis of porous channel flow with cross-diffusion, *American Journal of Computational and Applied Mathematics* 9 (5) (2019) 119–132.
- [23] Oahimire, J. I., Olajuwon, B. I., Waheed, M. A., Abiala, I. O., Analytical solution to MHD micropolar fluid flow past a vertical plate in a slipflow regime in the presence of thermal diffusion and thermal radiation, *Journal of the Nigerian Mathematical Society* 32 (1–3) (2013) 33–60.
- [24] Roache, P. J., The method of manufactured solutions for code verification, In: *Computer Simulation Validation*, Springer, 2019, pp. 295–318. https://doi.org/10.1007/978-3-319-70766-2_12
- [25] Salari, K., Knupp, P., Code verification by the method of manufactured solutions, Technical report SAND2000-1444, Sandia National Laboratories, Albuquerque, 2000.
- [26] Samarskii, A. A., The theory of difference schemes, CRC Press, 2001. <https://doi.org/10.1201/9780203908518>
- [27] Sharma, R., Ishak, A., Numerical simulation of transient free convection flow and heat transfer in a porous medium, *Mathematical Problems in Engineering* 2013 (2013) 1–9. <https://doi.org/10.1155/2013/371971>

- [28] Toro, E. F., Riemann solvers and numerical methods for fluid dynamics: A practical introduction, Springer, 1999. <https://doi.org/10.1007/978-3-662-03915-1>
- [29] Toro, E. F., Shock capturing methods for free-surface flows, Wiley, 2001.
- [30] Vafai, K., Kim, S. J., Forced convection in a channel filled with a porous medium: An exact solution, ASME Journal of Heat Transfer 111 (4) (1989) 1103–1106. <https://doi.org/10.1115/1.3250779>
- [31] Weli, A., Amadi, C. P., Nwaigwe, C., Numerical investigation of transport in a Couette flow with unsteady suction, IOSR Journal of Mathematics 15 (6) (2019) 74–83.
- [32] Weli, A., Nwaigwe, C., Numerical analysis of channel flow with velocity-dependent suction and nonlinear heat source, Journal of Interdisciplinary Mathematics 23 (5) (2020) 987–1008. <https://doi.org/10.1080/09720502.2020.1748278>